LASER APPLICATIONS AND OTHER TOPICS IN QUANTUM ELECTRONICS

Laser microphotoacoustic sensor of ammonia traces in the atmosphere

D.V. Serebryakov, I.V. Morozov, A.A. Kosterev, V.S. Letokhov

Abstract. **A microphotoacoustic highly selective sensor of ammonia is built. Main attention is paid to the operation mechanism of the acoustic sensor based on a quartz tuning fork. The optimal dimensions and configuration of the acoustic resonator are determined, which made it possible to increase the sensor sensitivity by two – three times compared to the sensitivity of the existing devices. The detector sensitivity for ammonia was 60 ppb (0.05 mg m^{-3}) for the measurement time of 10 s and a 25-mW, 1.53-μm laser beam in the acoustic resonator.**

1. Introduction

Laser photoacoustic spectroscopy [1, 2] is a well-established method for detecting microscopic quantities of chemical substances in gases. The method is based on detecting sound waves generated by a medium absorbing optical radiation. An important advantage of this method compared to other methods of analytic spectroscopy is the absence of a spectrally selective photodetector. However, this method has also significant disadvantages preventing its use outside laboratories. The main disadvantage of the method is its high sensitivity to the external acoustic noise, which makes the employment of these detectors problematic in the industrial environment.

In 2002, Kosterev and co-authors [3] proposed the design of a photoacoustic sensor based on a quartz piezoelectric tuning fork used as a master frequency oscillator in electronic watches. (These tuning forks have the oscillation eigenfrequency in vacuum equal to 32768 Hz, which determines the working frequency of the devices based on them.) The measurement technique utilising such a sensor was called quartz-enhanced photoacoustic spectroscopy (QEPAS). The described sensor is immune to external acoustic noises, compact, and its sensitivity threshold is determined by the thermal noises of the tuning fork. In addition, the quartz tuning fork has a huge linear dynamic

range – above 10^6, which allows the measurement of the gas concentrations from the detection limit up to 100% directly without adjusting the laser and without optical attenuators. The development of the semiconductor laser technology and, in particular, the availability of low-cost, near-IR, distributed-feedback (DFB) high-power single-frequency diode lasers eliminated the problems related to the cost, weight, and size of lasers. Thus, the QEPAS method in combination with modern diode lasers allows the fabrication of low-cost analytic devices for wide applications in industry, medicine, and other fields. This method and its use for the chemical analysis of gases are described in detail in paper [4].

In this paper, we describe the device for detecting the ammonia traces in the atmosphere. The device has an optimised acousto-optic cell enhancing the sensitivity of the method.

2. Description of the device

The basic diagram of the device is shown in Fig. 1. As a spectroscopic source, we used a Furukawa FOL-15TCWB-A tunable diode DFB laser with a fibre output in the 14-pin butterfly package. The optical radiation power at the sensor collimator output with this laser was about 25 mW. The laser was tuned to the ammonia absorption line by using two stabilisation systems, by temperature and current. The temperature was stabilised with a relative accuracy and reproducibility no worse than 5×10^{-3} °C, which ensures the close proximity of the laser radiation frequency and the absorption line when the system is switched on. The frequency is finely tuned and locked at the absorption line centre by using a feedback loop for which the source of the error signal is an InGaAs photodiode located after a reference cell with a high concentration of ammonia. Only a small fraction of laser radiation (about 1 %) is directed through the cell. The third harmonic of the laser modulation frequency is selected from the photodiode signal by a synchronous detector. This signal vanishes when the laser frequency and the absorption line maximum coincide.

The laser diode current is modulated by a sine signal at the frequency equal to the half the resonance frequency of the tuning fork. The modulation depth does not exceed 10 % of the mean current of the laser diode. The change in the current, apart from the change in the power, leads to a shift in the radiation wavelength. The direct modulation of the power caused by the change in the current virtually does not have high harmonics. At the same time, the wavelength-modulated radiation incident on the spectrally selective

D.V. Serebryakov, I.V. Morozov, V.S. Letokhov Institute for Spectroscopy, Russian Academy of Sciences, ul. Fizicheskaya 5, 142190 Troitsk, Moscow region, Russia; e-mail: serebr@isan.troitsk.ru;
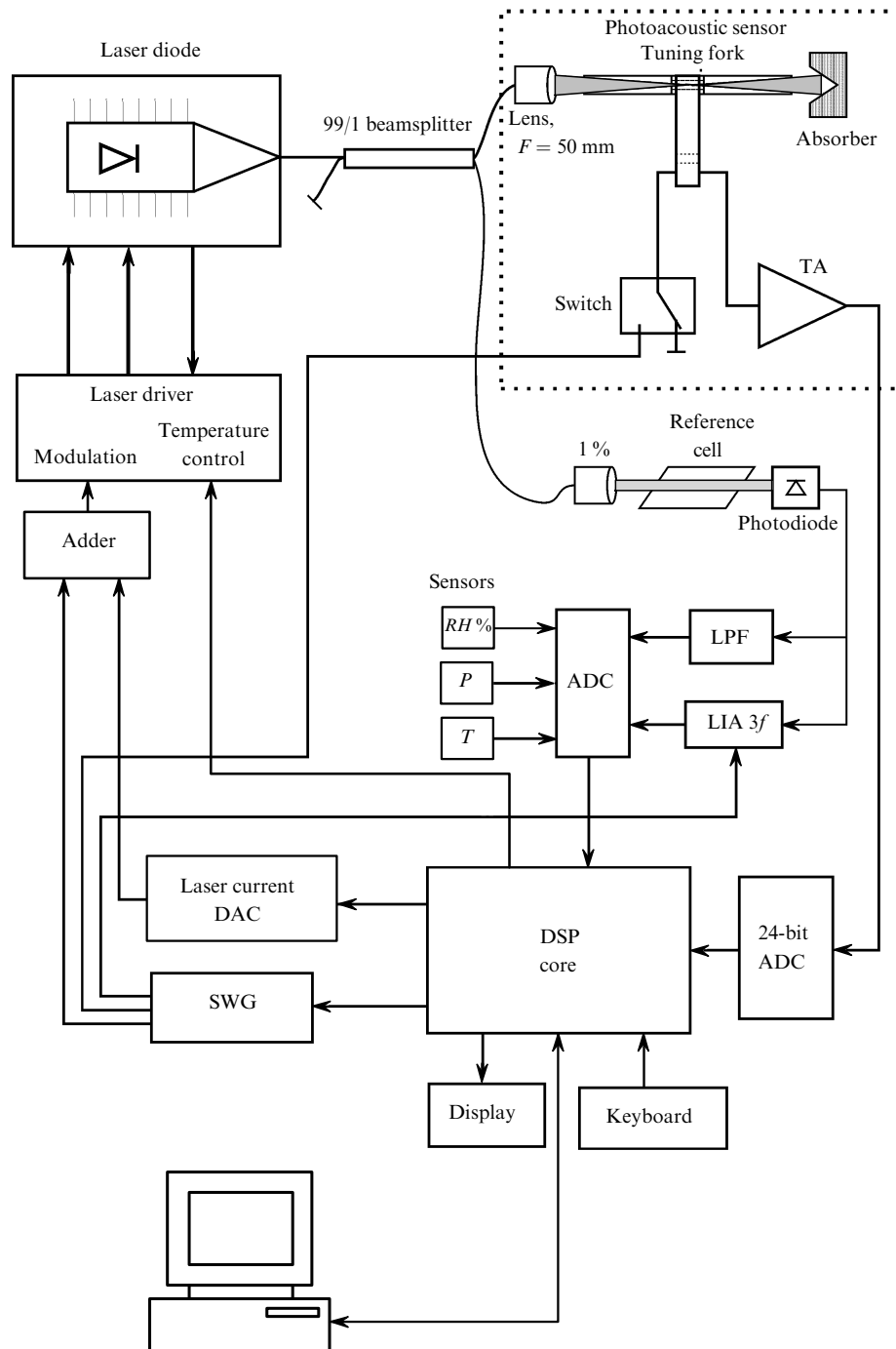**A.A. Kosterev** Rice Quantum Institute, Rice University, Houston, Texas 77251-1892

Figure 1. Scheme of the device: (SWG) sine wave generator; (LPF) low-pass filter; (LIA 3*f*) lock-in amplifier of the third harmonic of the modulation frequency; (TA) transimpedance amplifier; (*RH* %, *P*, *T*) humidity, pressure, and temperature sensors.

absorber generates a nonsine periodic signal containing high harmonics. This effect forms the basis of the modulation spectroscopy and makes it possible to realise in our case the advantages of the quartz tuning fork used as a microphone. The tuning fork has a high Q factor (when used in the sensor, it is in the range from 3000 to 2000, depending on the gas pressure and the tuning fork configuration); therefore, the tuning fork is almost insensitive to sound oscillations at the modulation frequency, which are caused by the nonselective absorption of laser radiation in the gas and by heating of the cell elements by stray radiation. The tuning fork detects sound oscillations, caused by the double

intersection of the absorption line by the laser line during the modulation period, only at the second harmonic of the modulating frequency. This also provides a high selectivity of the method because the appearance of the acoustic signal requires the coincidence of the absorption line with the reference line to which the central laser optical frequency is locked.

The signal from the quartz tuning fork is amplified by a current – voltage converter (an amplifier with the zero input resistance) and is digitised in a high-speed 24-bit analogue-to-digital converter (ADC). The digitised signal is filtered and the second harmonic of the modulation signal, in-phase

with the photoacoustic signal, is selected from it. The second-harmonic signal is normalised to the laser average power, which is determined by the average photodiode current measured with the help of the low-pass filter (LPF), and to the quartz tuning fork Q factor determining the sensor response.

The direct digital signal processing, unlike the analogue synchronous detection used in paper [4], allows one to completely eliminate the zero drift caused by the change in the temperature and by the component ageing. There remain an insignificant offset caused by the pick-up of the laser current modulation harmonics into the measurement channel; however, according to our experience, the electric noises can be suppressed down to an arbitrarily low level. The use of the 24-bit ADC makes it possible to retain the large dynamic range of the device.

During the self-calibration, the tuning fork is connected to the sine signal generator with the help of an electronic key, the laser frequency is detuned from the frequency of the absorption line by the preliminary set quantity, and the resonance frequency, Q factor, active resistance of the tuning fork are measured, while the zero offset of both the measurement channel and the channel of the laser line locking are compensated for. The operation of the described device is presented in detail in paper [4].

This device has embedded temperature, humidity, and pressure sensors registering the measurement condition as well as a clock and a nonvolatile Flash memory allowing one to log the results for several days without using an external PC. The optical design of the device is based on fibreoptic elements, similarly to [5].

In the experiments, we used the 1531.68-nm laser radiation wavelength. Near this wavelength there is a group of three absorption lines of ammonia, which are overlapped at the atmospheric pressure and provide the maximum absorption in the 1525–1610-nm range accessible by telecommunication lasers (Fig. 2). The characteristic feature of this absorption line is almost constant detection sensitivity in the case of significant changes in the ammonia pressure. The ammonia detection technique utilising the described sensor is described in detail in paper [6].
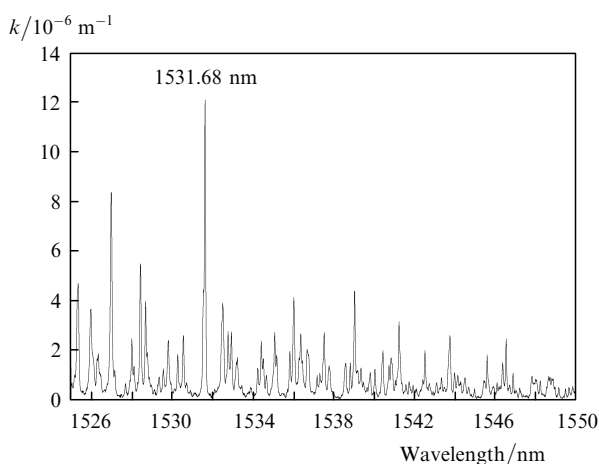

Figure 2. Spectrum of the ammonia absorption coefficient in the telecommunication range [according to the PNNL (USA) data] when its content in air is 1 ppm, the length of the optical path is 1 m and the temperature is 296 K. The absorption coefficient k is determined from the ratio $k = \lg(1/T)/L$, where T is the transmission coefficient.

3. Photoacoustic detector

Figure 3 presents the photograph of the photoacoustic sensor and its characteristic dimensions. The diameter of the acoustic amplifier tube (0.4 mm) was chosen to be close to the distance between the tuning fork prongs. The gaps between the tube surfaces and the tuning fork were 0.05–0.1 mm. The decrease in the gaps leads to a significant increase in the losses in the tuning fork due to viscous drag in the boundary air layer, to a decrease in the tuning fork Q factor and, hence, to a decrease in the sensitivity of the device (signal-to-noise ratio at the given concentration of the measured gas in air). An increase in the gaps (more than 0.1 mm) leads to a decrease in the 'amplification coefficient' of the tube.
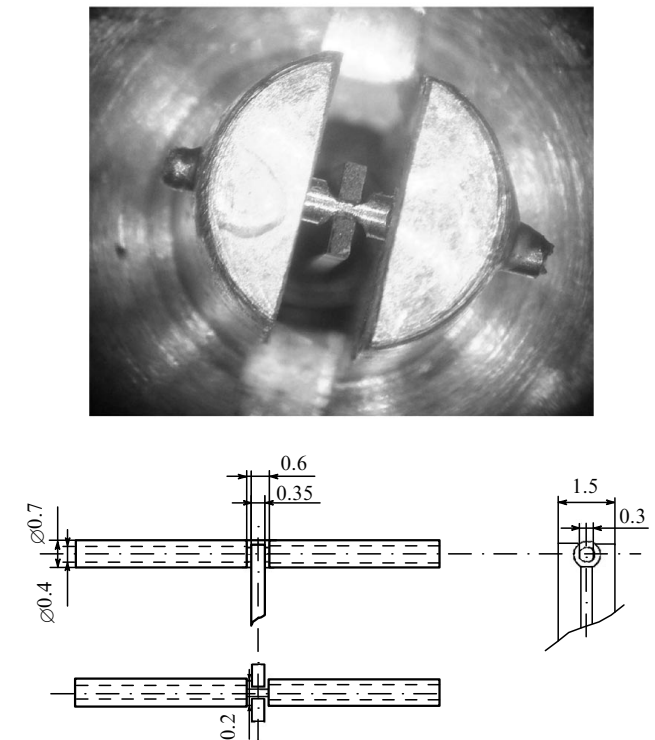

Figure 3. Photoacoustic sensor and its characteristic dimensions (in mm).

The quartz tuning fork has the maximum sensitivity to the external force when it is applied to the upper edge of the prongs. This problem was described in detail, for example, in paper [7]. The optimal position of the laser beam waist (from top to bottom) in the tuning fork gap for detecting the photoacoustic signal was analysed in paper [8].

The authors of papers [3–6] used the tubes of total length ~ 5 mm. This design allowed the signal amplification approximately by a factor of ten compared to the case when only the tuning fork was used (Fig. 4b). In this case, there was observed some decrease in the tuning fork Q factor: from 12000–14000 to 9500–10000. The presence of the bridges between the two halves of the tube leads to the further decrease in the Q factor down to ~ 8500; however, the sensitivity increased approximately by 1.3 times in this case.

The increase in the sensitivity is explained by the growth of the sound wave pressure through a decrease in the
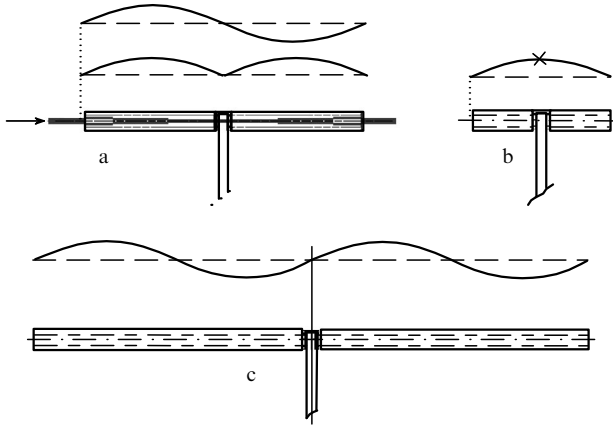
Figure 4. Pressure distribution of natural oscillations in tubes with a hole in the middle for the tube length equal to the sound wavelength λ (a, upper curve), for the tube length $\lambda/2$ (in the case of a hole in the tube centre, the pressure antinode is impossible in this place, which is shown in the figure) (b), and for the tube length 2λ (c), as well as the pressure distribution during the excitation of the oscillations by heating the gas by a laser beam (a, lower curve).

scattering of the acoustic oscillation energy from the gap between the tuning fork prongs and not by the resonance effect in the tube, as for example the case in paper [9]. The resonance phenomenon in this tube configuration is excluded in accordance with the classical theory of the sound oscillations (see, for example, [10]) because the presence of even a small hole in it makes the formation of the pressure antinode impossible and, hence, 'prohibits' the resonance oscillations with the wavelength twice greater than the tube length. In our case, the hole is by no means small, and the total area of the gaps in the place where the tuning fork is mounted is ~ 0.31 mm^2, which is approximately 2.5 times larger than the area of the tube cross section.

For a tube with a hole in the middle, free oscillations with an integer of the half-waves are allowed (see, for example, Figs 4a, c). However, when the source term is homogeneous, i.e. the gas is heated by a laser beam simultaneously along the tube length, the oscillation mode shown in Fig. 4c is not excited (if we neglect the edge effects which can result in the existence of this oscillation mode however with the amplitude smaller than that determined by the simple gas heating in the tube) because the presence of both excees and reduced pressure regions is needed for its existence. The gas heating by the laser beam leads to a pressure increase along the entire tube simultaneously. In tube presented in Fig. 4a, oscillations can appear (lower curve) in the presence of strong dissipation in the central hole.

To test this hypothesis, it was necessary to study experimentally the dependence of the device sensitivity on the tube length. In this case, the significant initial scatter in the parameters of different photoacoustic sensors, caused by the different position of the tuning fork in the tube gap and the shape of the central hole, as well as the complexity of manufacturing of each sensor should be taken into account. Therefore, we developed a technology of grinding off the tube ends of a sensor with the help of a diamond tool, whose employment did not lead to the displacement of the tuning fork and, as a result, to the change in the device parameters not related to the tube length.

The measured dependence of the tuning fork Q factor on the tube length are presented in Fig. 5.

The speed of sound in the tube in the general case differs from that in free medium. In addition, there exist so-called Rayleigh (end) lengthening corrections [10] for the effective tube length in the resonance, which are equal to 0.6 of the tube radius for its each end. The tuning fork positioned in the tube centre may also have an impact on its effective length.
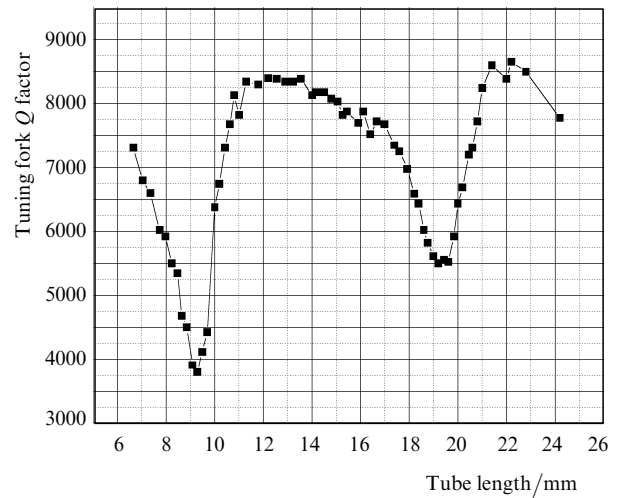

Figure 5. Dependence of the tuning fork Q factor on the tube length.

Because we know the exact position of the minima in Fig. 5 (maximum losses in the tuning fork correspond to the tuning fork eigenfrequency equal to 32758 Hz), we obtain two linear equations (one for the second oscillation mode and one for the fourth oscillation mode) in two unknowns – the speed of sound and the difference between the real and effective tube lengths. It follows from the solution of these equations that the speed of sound in the tube is 331 m s^{-1}, and its effective length is larger than the real one by 0.82 mm. The Rayleigh end corrections make up 0.24 mm for the ordinary tube end and 0.33 m for the tube with flanges. Because there is a significant discrepancy between the results of the calculations and the experiment, we performed a test experiment by placing flanges on the tube ends. In this case, the effective length increased approximately by 0.1 mm, which corresponds to the difference between the Rayleigh corrections. Therefore, we can conclude that the necessity for an additional shortening of the tube by 0.58 mm is explained by the influence of the central hole and acoustic coupling to the tuning fork. We can also estimate the energy losses caused by the viscous friction of the gas on the tube walls and radiation from its ends. These losses are calculated by using the expressions [10]

$$Q = \left(\frac{3}{2} \frac{\omega\rho}{\eta} \right)^{1/2} r \approx 29, \tag{1}$$

$$\Delta P = \frac{4k^2 S}{\Omega} \approx 0.015, \tag{2}$$

where Q is the acoustic resonator Q factor determined by the losses on the walls; $\omega \approx 2 \times 10^5$ s^{-1} is the circular

frequency of the acoustic oscillations; $r = 0.2$ mm is the tube radius; $\rho = 1.2$ kg m^{-3} is the air density; $\eta = 1.722 \times 10^{-5}$ Pa s is the air viscosity coefficient; $k \approx 620$ m^{-1} is the wave number; $S = 7 \times 10^{-8}$ m^2 is the area of the tube cross section; $\Omega = 4\pi$ is the solid angle of radiation; ΔP is the power loss during the reflection of the wave from the tube end. The losses by 1.5 % correspond to $Q = 400$ for the tube length λ and $Q = 800$ for the tube length 2λ. Thus, the resulting Q factor of the tubes without holes in the middle, taking into account these basic factors, will be 27.3 and 28.2, respectively.

To determine the actual Q factor, it is necessary to recalculate the dependence of the Q factor on the tube length (Fig. 5) into the dependence of the attenuation being introduced at the resonance frequency of the tube (Fig. 6). Because when the tube length is changed, the equivalent wave resistance Z of the resonator ($Z_{eq} = \rho v / S$, where v is the sound speed [10]) as well as the active losses and the coupling coefficient between the tuning fork and the resonator at the measurement frequency (the resonance frequency of the tuning fork) are retained, the curves in Fig. 6 are equivalent to the dependence of the active losses on the frequency at the constant tube length. We can explain it by the example of the classical frequency-tunable circuit (in this case, it is necessary to change the circuit capacity and inductance proportionally to the detuning of the frequency f from f_0) while retaining the Q factor and the wave resistance; for such a contour the total resistance is

$$Z = R + 1/[j\omega f(C_0/f_0)] + j\omega f(L_0/f_0), \qquad (3)$$

where ω is the frequency at which Z is measured; R is the active resistance of the contour; f is the current resonance frequency of the contour; C_0 and L_0 are the contour capacity and inductance at the resonance frequency f_0. It is obvious that the dependences of Z on ω and f are identical. The same is valid in our case: in equations describing the equivalent scheme of the acoustic resonator all the impedances of the reactive elements will depend on the product ωf.

The resonance curves in Fig. 6 have a strongly pronounced asymmetry; therefore, measuring the Q factor simply by the peak half-width yields a larger error. However, the same frequency dependence of the active component of the resistance is typical of the electric circuit shown in Fig. 7. The additional element C_2 is responsible for the asymmetry of the resonance characteristic. We can approximate the curves in Fig. 6 by using the expression

$$R_{act} = \mathrm{Re}\left\{ \frac{\left[\dfrac{j\omega L(1/j\omega C_1)}{j\omega L + 1/j\omega C_1} + 1/j\omega C_2 \right] R}{\dfrac{j\omega L(1/j\omega C_1)}{j\omega L + 1/j\omega C_1} + 1/j\omega C_2 + R} \right\} \qquad (4)$$

and, based on the obtained parameters of the equivalent circuit elements, we can calculate the Q factor. The results of the approximation are shown in Figs 6a, b by dashed curves. The Q factors in this case were 7.25 and 11.1, respectively.

To check the obtained results, we can compare two ratios – the calculated Q factors and the minima of the tuning fork Q factors (see Fig. 5). These ratios should be identical because nothing changes in the system except for the tube length, and the changes in the tuning fork Q factor should correspond to the change in the total losses in the
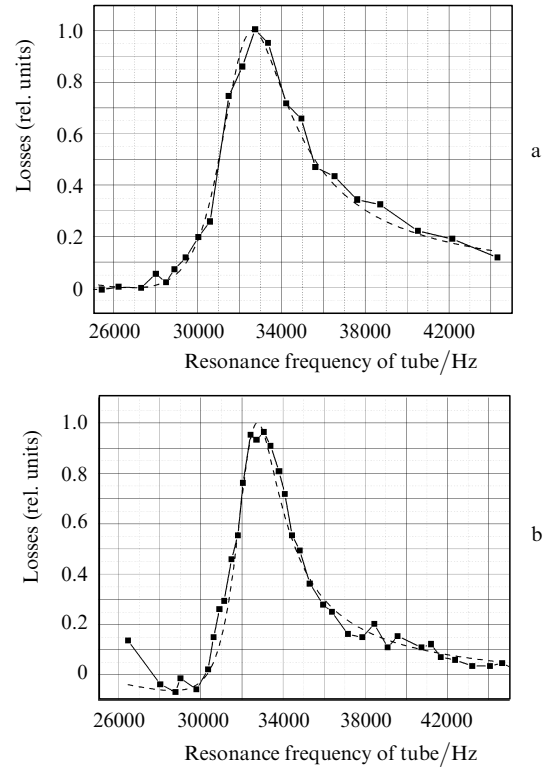

Figure 6. Dependences of the losses in the tuning fork on the resonance frequency of the tube for the second (a) and fourth (b) oscillation modes: the results of the experiment (points) and simulation (dashed curves) at $Q = 7.25$ (a) and 11.1 (b).
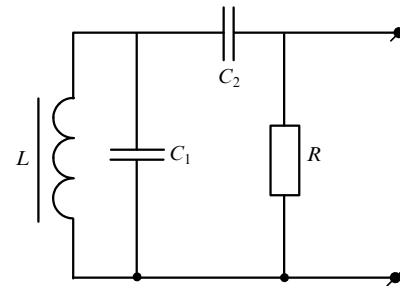

Figure 7. Equivalent circuit of the oscillation system.

oscillation system. The ratios of the Q factors are 1.54 for the calculated parameters and 1.45 – for the tuning fork. The discrepancy is 6 %, which allows the conclusion about the correctness of calculations of the acoustic resonator Q factors.

Now we can calculate the energy losses in the tube caused by the hole in its centre. The contribution of these losses to the total losses in the case of the second-order oscillations is $\Gamma_2 = 7.25^{-1} - 27.3^{-1} \approx 0.101$, and in the case of the fourth-order oscillations, this contribution is equal to $\Gamma_4 = 11.1^{-1} - 28.2^{-1} \approx 0.054$ (the losses are inversely proportional to the Q factor) and is dominating. The theoretical ratio of these losses should differ exactly twofold (the ratio of the effective tube lengths). In our case, it is equal to 1.87, i.e. only 7 % lower than the theoretical. Therefore, we can expect that the highest sensitivity of the sensor will be observed for the tube length slightly shorter than λ. This is confirmed in practice (Fig. 8): the maximum signal is

observed for the tube length 9.3–9.4 mm. (The measurements were performed using the Chromdet GEA-01 ammonia generator intended for calibrating the industrial ammonia sensors.) Based on this, further improvement of the sensitivity due to the optimisation of the tube dimensions is hardly possible because the shape of the hole for the tuning fork, as was noted above, is bounded by the necessity to avoid losses in the boundary layer of the air and cannot be smaller than 30 μm.
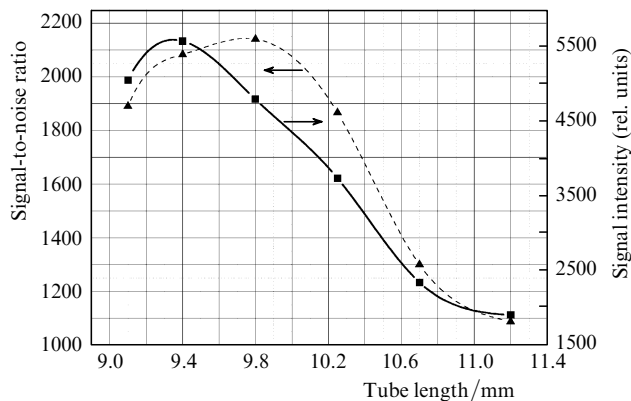

Figure 8. Dependences of the sensor signal intensity and the resulting signal-to-noise ratio with the averaging time 10 s on the tube length. The ammonia content is 100 mg m^{-3}.

4. Conclusions

The use of a tube of 'resonant' length allows one to approximately double the sensor sensitivity; however, this also has a negative effect: a decrease in the tuning fork Q factor and an increase in the active resistance of the tuning fork, which is proportional to this decrease, lead to a drop in the signal-to-noise ratio as $\sqrt{Q_{tf}}$ at a fixed sound pressure. (The amplitude of the tuning fork oscillations and, consequently, the current generated by this tuning fork decreases linearly with decreasing Q_{tf}, the noise current also decreasing but as $\sqrt{Q_{tf}}$ [7].) Therefore, the increase in the sensitivity is not so significant. In addition, the low Q factor of the tuning fork broadens its passband, making the tuning fork more sensitive to external acoustic noises.

The experimentally measured sensitivity to ammonia in the case of the optimal geometry of the acoustic resonator (of length 9.4 mm and diameter 0.4 mm) is 0.047 mg m^{-3} or 0.06 ppm for the signal averaging time equal to 10 s and the signal-to-noise ratio equal to unity, which can be recalculated to NNEA = 3.3×10^{-9} cm^{-1} W Hz$^{-1/2}$ (NNEA is the normalised noise equivalent absorption coefficient). This value is 1.5 times worse than the value obtained with the help of the 'classical' photoacoustic method for ammonia detection at the 1800-Hz frequency [11], which was equal to 2.2×10^{-9} cm^{-1} W Hz$^{-1/2}$. In this case, the optical path in the optoacoustic cell was 184 mm, which is 20 times more than in the device described in the present paper.

When the cavity ring down spectroscopy is used, the sensitivity proves to be higher. For example, when the ammonia concentration was measured at the same wavelength for the 650-mm-long resonator with a diameter of 25 mm [12], the sensitivity of 1.06×10^{-9} cm^{-1} W Hz$^{-1/2}$ is

achieved. When the multipass method was used, the sensitivity is only 40×10^{-9} cm^{-1} W Hz$^{-1/2}$ for the optical path of 36 m [13].

The systems described in [11–13] and their counterparts have significantly larger characteristic dimensions of the measuring elements (tens of centimetres) and are highly sensitive to acoustic and vibrational noises, while the methods described in [12, 13] impose the highest requirements to the quality of the mirrors being used and to the retention of this quality during the operation life of the device. All this substantially complicates the fabrication of the production samples of measurement devices based on the above-mentioned methods with the sensitivity close to that obtained in the laboratory. The measuring element described in this paper has the characteristic dimensions of about 50 mm, is highly immune to acoustic noises, has a high chemical resistance, long service life, and does not need adjustment during the entire operation life.

The sensitivity of the quartz microphotoacoustic sensor per optical path length is tens times higher than that of other methods for detecting gas traces. This makes it possible to design sensors having the sensitivity similar to other highly sensitive detection methods employing diode near-IR lasers. At the same time, the microphotoacoustic sensor is free from the drawbacks inherent in the above-mentioned methods preventing the fabrication of the systems suitable for real-world applications.

References

1. Zharov V.P., Letokhov V.S. *Laser Optoacoustic Spectroscopy, Springer Series in Optical Sciences* (Berlin, Springer, 1986) Vol. 37.
2. Sigrist M.W. *Rev. Sci. Instrum.*, **74** (1), 486 (2003).
3. Kosterev A.A., Bakhirkin Yu.A., Curl R.F., Tittel F.K. *Opt. Lett.*, **27**, 1902 (2002).
4. Kosterev A.A., Tittel F.K. Serebryakov D.V., Malinovsky A.L., Morozov I.V. *Rev. Sci. Instrum.*, **76** (4), 043105 (2005).
5. Kosterev A.A., Mosely T.S., Tittel F.K. *Appl. Phys. B*, **85**, 295 (2006).
6. Kosterev A.A., Tittel F.K. *Appl. Opt.*, **43**, 6213 (2004).
7. Serebryakov D.V., Cherkun A.P., Loginov B.A., Letokhov V.S. *Rev. Sci. Instrum.*, **73**, 1795 (2002).
8. Petra N., Zweck J., Kosterev A.A., Minkoff S.E., Thomazy D. *Appl. Phys. B*, **94**, 673 (2009).
9. Bijnen F.G.C., Reuss J., Harren F.J.M. *Rev. Sci. Instrum.*, **67** (8), 2914 (1996).
10. Pippard A.B. *The Physics of Vibration* (London: Cambridge University Press, 1978).
11. Webber M.E., Pushkarsky M., Kumar C., Patel N. *Appl. Opt.*, **42**, 2119 (2003).
12. Peeters R., Berden G., Apituley A., Meijer G. *Appl. Phys. B*, **71**, 231 (2000).
13. Claps R., Englich F.V., Leleux D.P., Richter D., Tittel F.K., Curl R.F. *Appl. Opt.*, **40**, 4387 (2001).